Electronic Supplementary Material (ESI) for Journal of Materials Chemistry A.

Supporting information:

High-Performance Piezoelectric Nanogenerators Featuring Embedded Organic Nanodroplets for Self-Powered Sensor

Hai Li[1], Sooman Lim[1,*]

[1] Department of Flexible and Printable Electronics, LANL-JBNU Engineering Institute, Jeonbuk National University, Jeonju, 54896, Republic of Korea

*Corresponding author: Prof. Sooman Lim; E-mail: smlim@jbnu.ac.kr

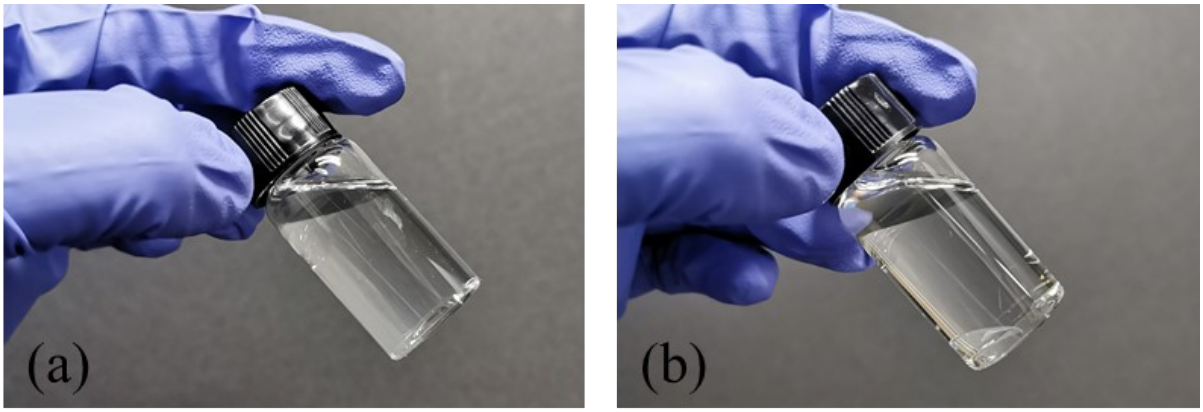

Figure S1. Digital photos showing the solubility of the FDTS in DMK solution (a) and DMF solution (b).

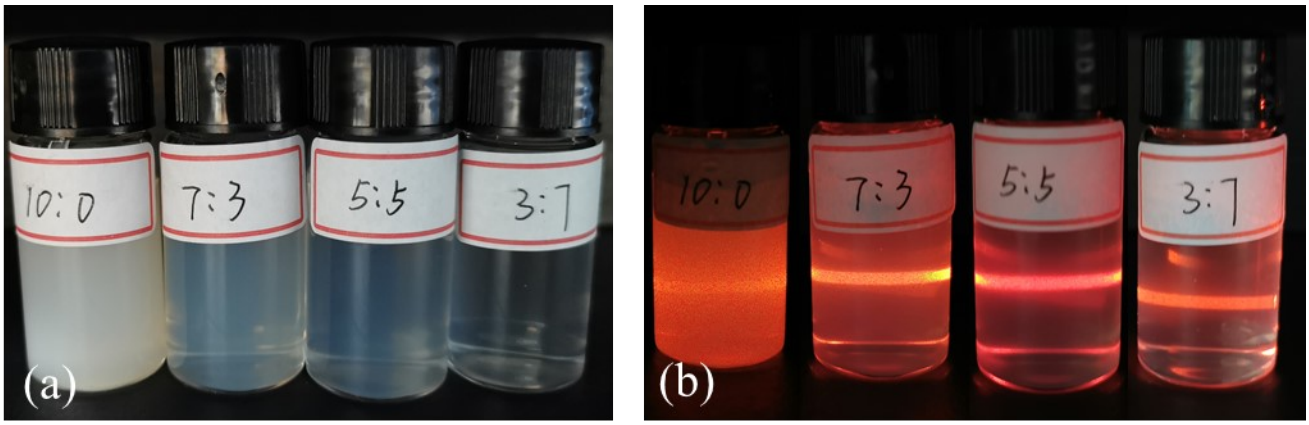

Figure S2. The photos of as-prepared emulsions (a) before and (b) after applying the laser beam illustrate the Tyndall effect.

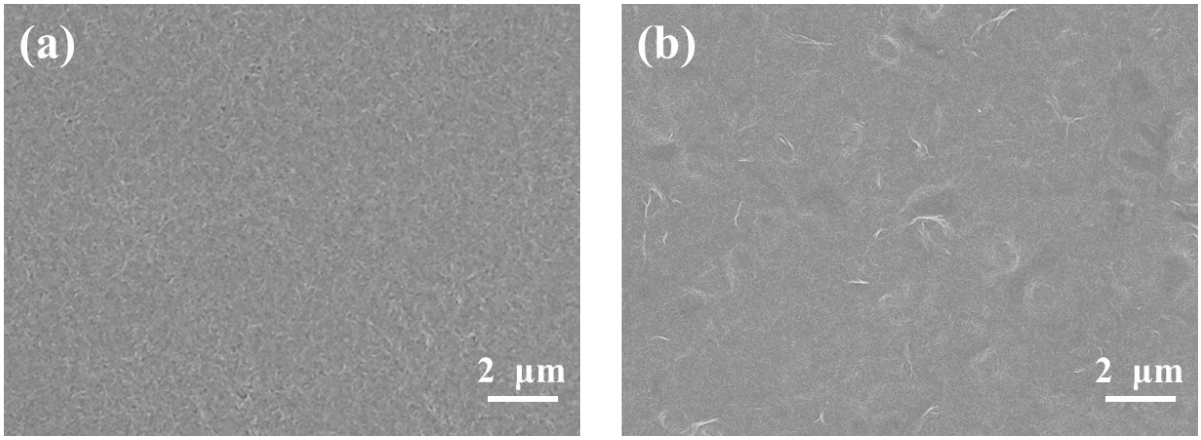

Figure S3. SEM images of the surface of the (a) pristine PVDF film and (b) PVDF-10% solid-liquid composite film.

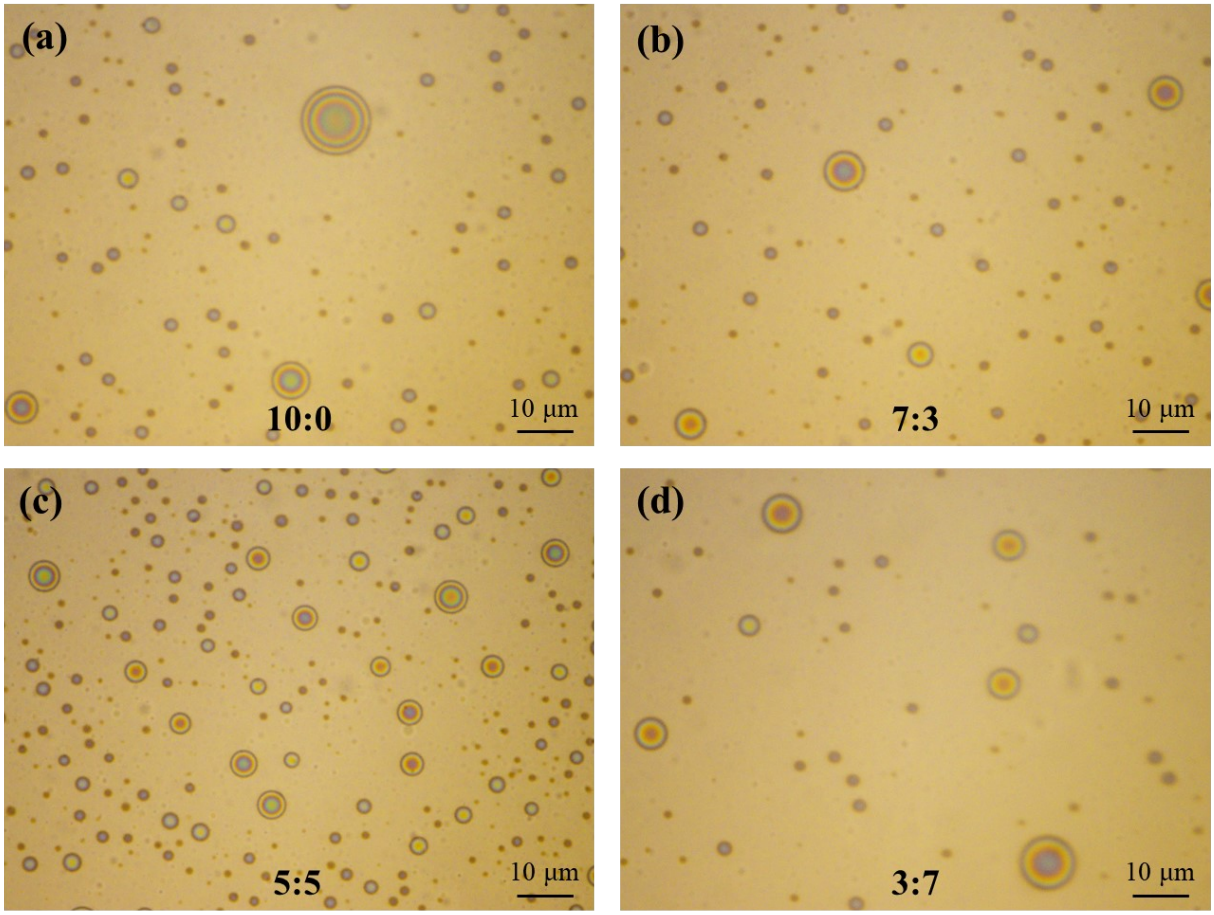

Figure S4. Optical micrograph images of the FDTS liquid state in emulsions of the DMF:DMK at (a) 10:0; (b) 7:3; (c) 5:5; (d) 3:7.

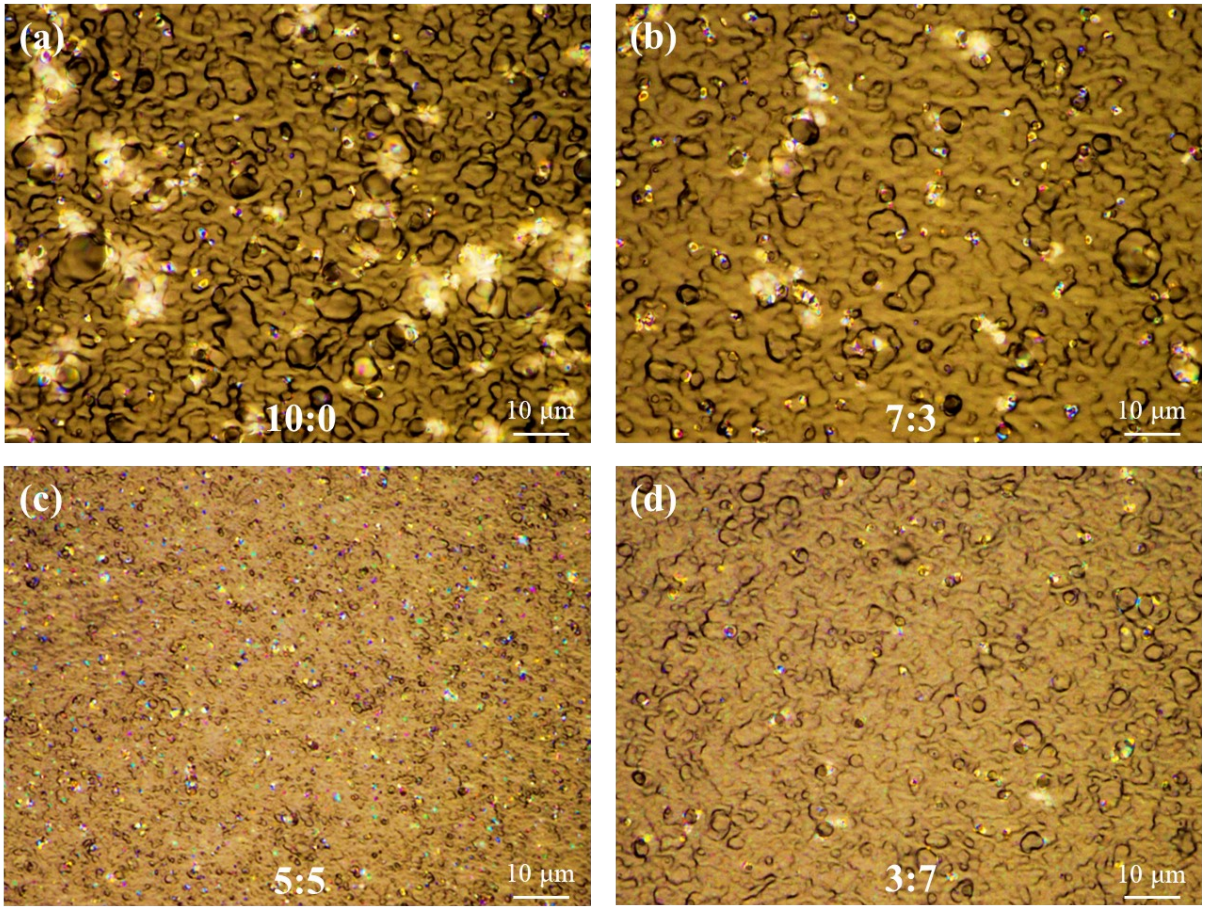

Figure S5. Optical micrograph image of the resultant dry film when the volume ratio of the DMF:DMK is (a) 10:0; (b) 7:3; (c) 5:5; (d) 3:7.

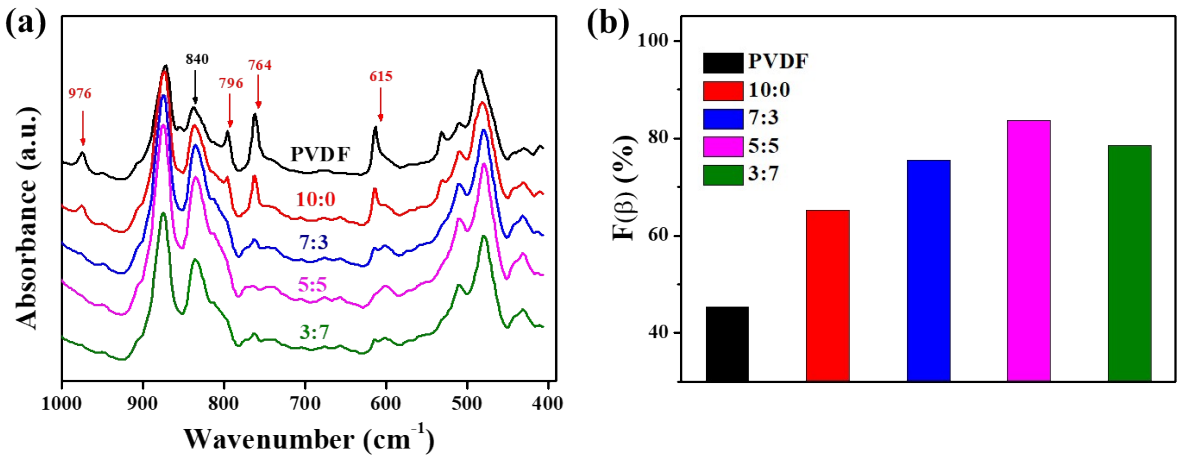

Figure S6. (a) FTIR spectra of the bulk PVDF film and solid–liquid nanocomposites prepared under different volume ratios of DMF:DMK. (b) The F(β) value variations in the bulk PVDF film and solid–liquid nanocomposites prepared under different volume ratios of DMF:DMK.

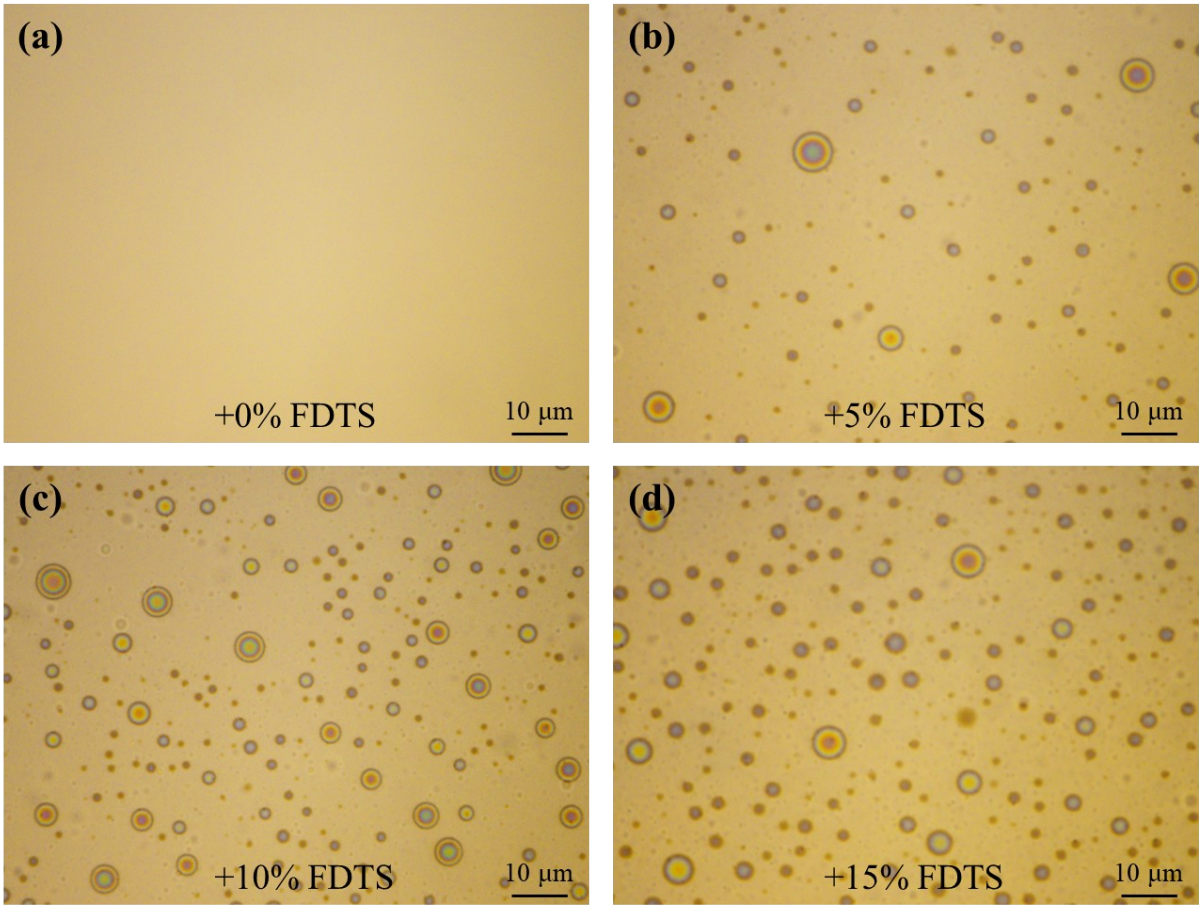

Figure S7. Optical micrograph images of the as-prepared emulsions with (a) 0 wt% FDTS, (b) 5 wt% FDTS, (c) 10 wt% FDTS, (d) 15 wt% FDTS.

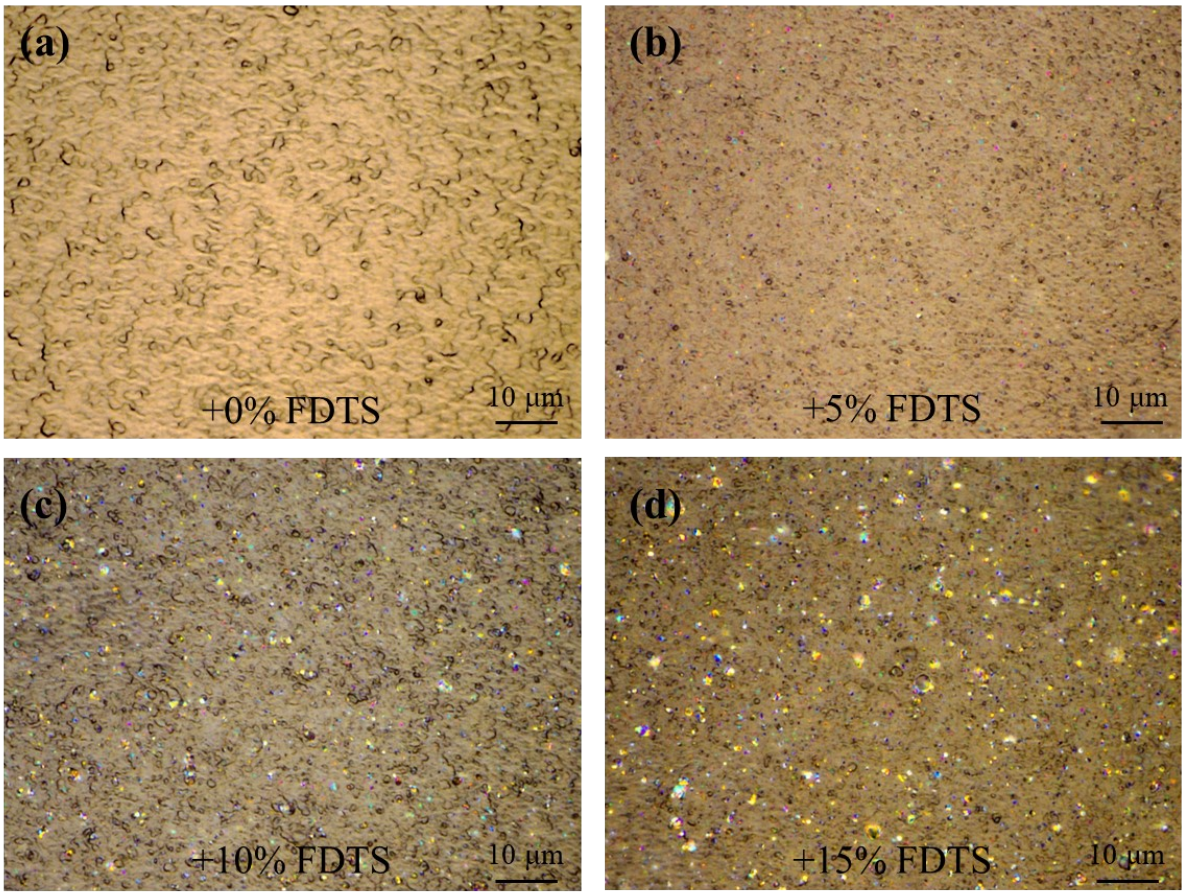

Figure S8. Optical micrograph image of the resultant dry film with (a) 0 wt% FDTS, (b) 5 wt% FDTS, (c) 10 wt% FDTS, (d) 15 wt% FDTS.

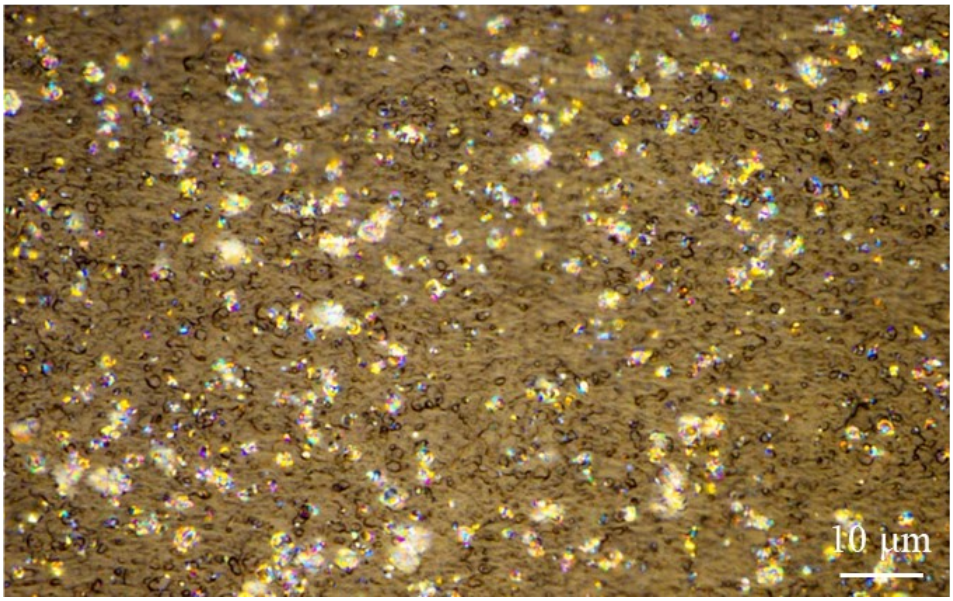

Figure S9. Optical micrograph image of the dry film with 20 wt% FDTS.

Table S1. Mechanical properties of as-printed films.

Sample details	Young's modulus (MPa)	Ultimate tensile strength (MPa)	Strain-to-failure (%)
PVDF	710.54±83	38.46±7.65	8.39±3.36
PVDF-5%	598.23±72	30.95±6.18	15.95±4.53
PVDF-10%	435.89±68	24.06±4.58	40.39±6.59
PVDF-15%	362.65±76	21.89±5.39	76.21±9.83

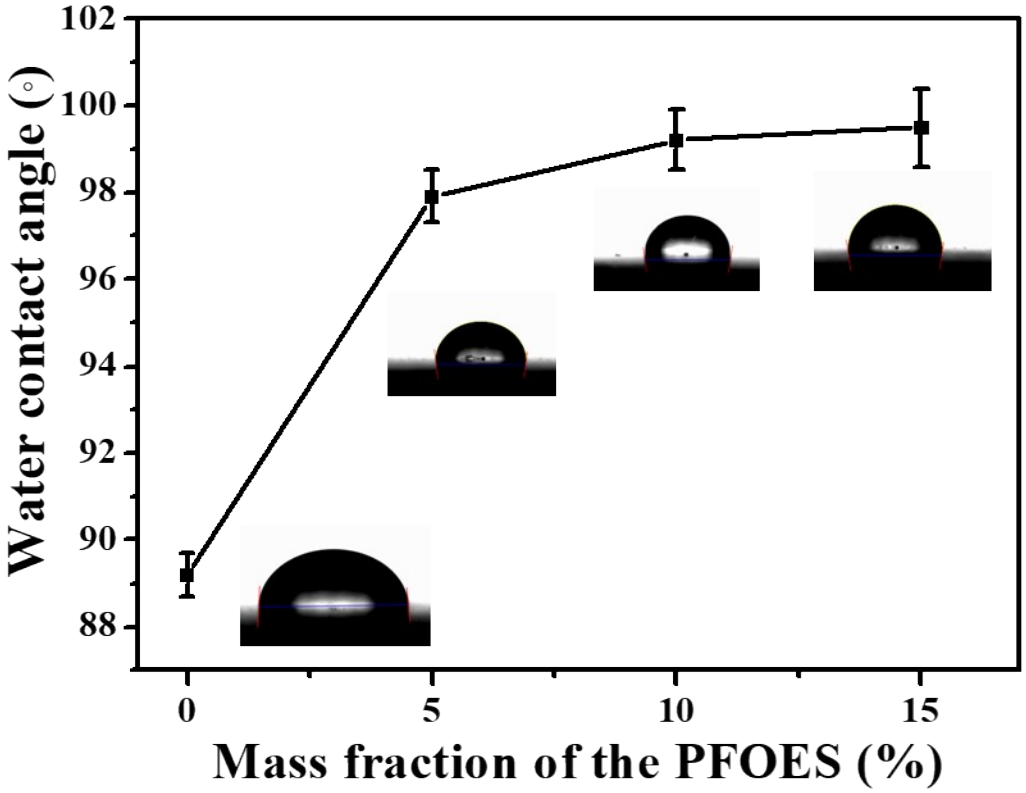

Figure S10. Contact angle of as-prepared emulsions with different contents of FDTS dropped on ITO-PET film.

Table S2. Calculated surface energies of as-prepared samples using the contact angles measured with two different solvents

Sample details	Water CA (degrees)	Diiodomethane CA (degrees)	Surface energy (mN m^{-1})	Dispersive surface energy (mN m^{-1})	Polar surface energy (mN m^{-1})
ITO-PET	88.2	43.3	38.02	36.42	1.59
PVDF-5%	97.9	55.7	28.68	25.43	3.25
PVDF-10%	99.2	56.4	29.72	26.58	3.06
PVDF-15%	99.5	58.1	31.01	28.07	2.94

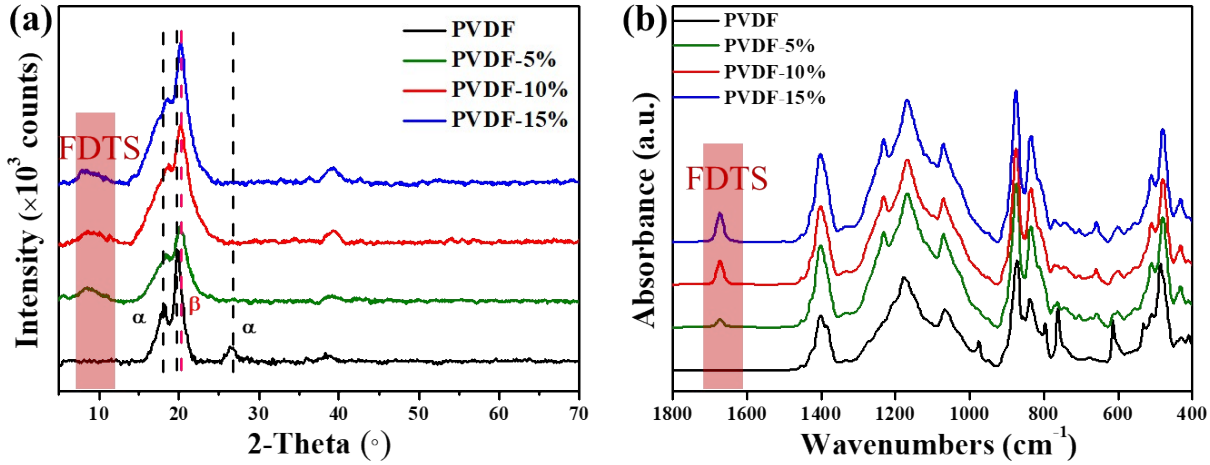

Figure S11. XRD and FTIR spectra of the as-printed the bulk PVDF film and solid–liquid nanocomposites.

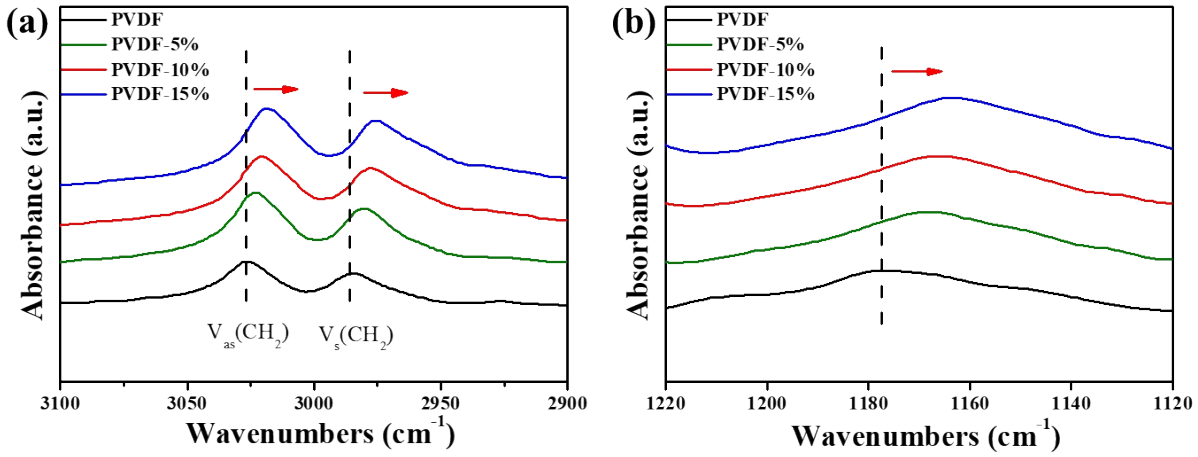

Figure S12. FT-IR spectra of the as-printed the bulk PVDF film and solid–liquid nanocomposites with a wavenumber range of (a) 3100 cm^{-1} to 2900 cm^{-1} and (b) 1220 cm^{-1} to 1120 cm^{-1}.

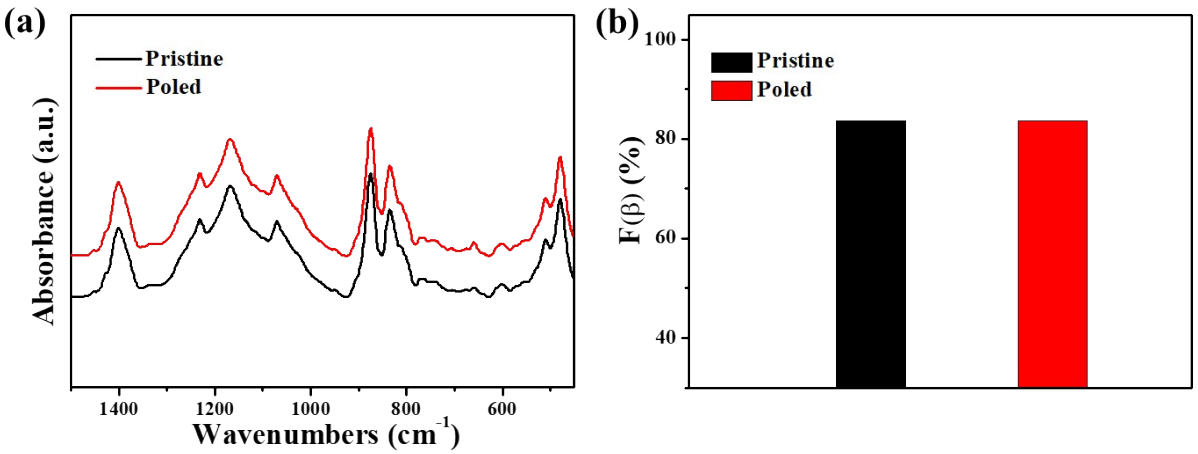

Figure S13. (c) FT-IR spectra of the as-printed solid–liquid nanocomposites with and without electric poling. (d) The F(β) values in the printed samples.

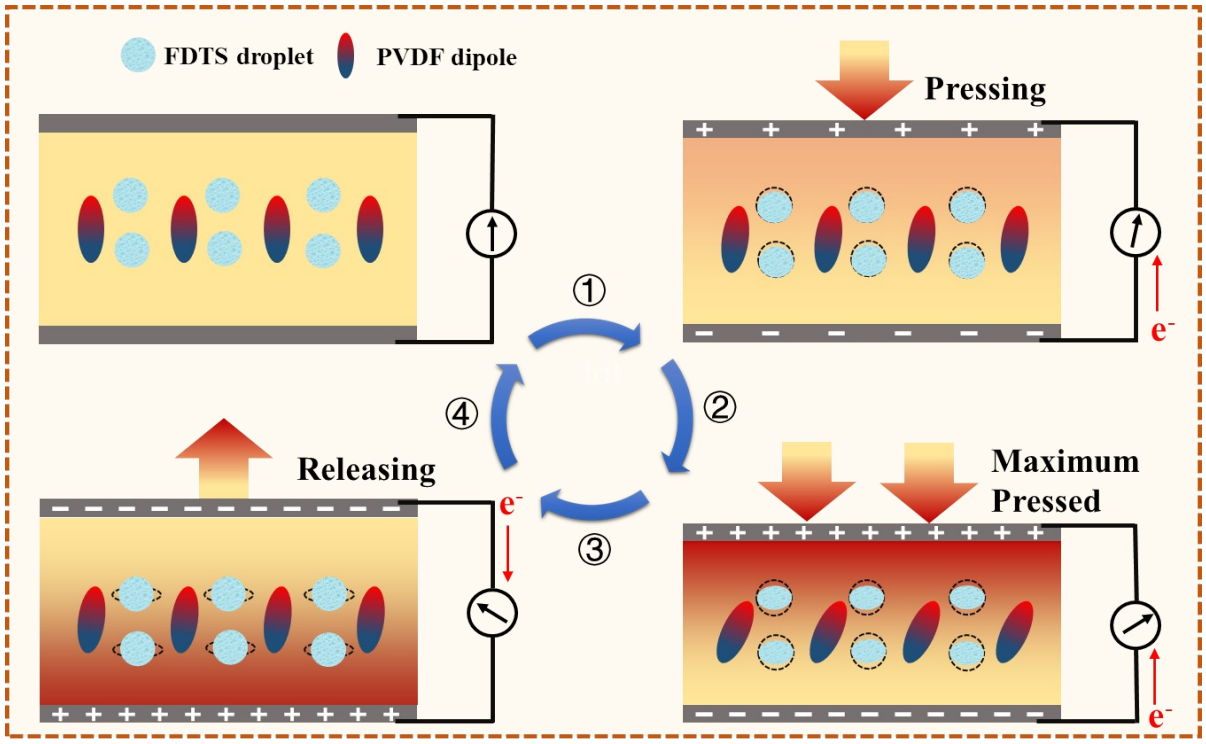

Figure S14. Schematic of the electron generation process in the solid–liquid nanocomposite.

Table S3. Summary of PVDF-based materials in our study and other reported studies.

Materials	Form	Working condition	Voltage	Power density	Sensitivity	Ref.
MXene/ PVDF	Porous film	0.1 MPa	1.5 V	0.13 μW/cm^2	11.9 nA/kPa	[1]
PVDF	Porous film	2G acceleration	40 V	012 μW/cm^2	None	[2]
$CH_3NH_3PbI_3$/ PVDF	Porous film	finger imparting	1.5 V	2.5 μW/cm^2	None	[3]
Ag nanowire/ PVDF	Porous film	10 N	23 V	7.1 μW/cm^2	None	[4]
$FAPbBr_2I$/ PVDF	Porous film	2G acceleration	42 V	10 μW/cm^2	None	[5]
P(VDF-HFP)	Porous film	0.36 MPa	9 V	11 μW/cm^2	1 μV/Pa	[6]
PVDF-TrFE	Porous film	0.2 MPa	21 V	28.5 μW/cm^2	None	[7]
BNNT/PVDF-TrFE	Micropillar arrays	0.4 MPa	22 V	11.3 μW/cm^2	55 V/MPa	[8]
BTO/PVDF-TrFE	Micropillar arrays	0.5 MPa	13.2 V	12.7 μW/cm^2	257.9 mV/N	[9]
FDTS/PVDF	Solid-liquid film	0.5 MPa	62 V	32.8 μW/cm^2	0.134V/kPa	This work

References

[1]. Kim J, Jang M, Jeong G, et al. MXene-enhanced β-phase crystallization in ferroelectric porous composites for highly-sensitive dynamic force sensors[J]. Nano Energy, 2021, 89: 106409.

[2]. Rana M M, Khan A A, Huang G, et al. Porosity Modulated High-Performance Piezoelectric Nanogenerator Based on Organic/Inorganic Nanomaterials for Self-Powered Structural Health Monitoring[J]. ACS Applied Materials & Interfaces, 2020, 12(42): 47503-47512.

[3]. Sultana A, Sadhukhan P, Alam M M, et al. Organo-lead halide perovskite induced electroactive β-phase in porous PVDF films: an excellent material for photoactive piezoelectric energy harvester and photodetector[J]. ACS applied materials & interfaces, 2018, 10(4): 4121-4130.

[4]. Zhou Z, Du X, Luo J, et al. Coupling of interface effects and porous microstructures in translucent piezoelectric composites for enhanced energy harvesting and sensing[J]. Nano Energy, 2021, 84: 105895.

[5]. Khan A A, Rana M M, Huang G, et al. Maximizing piezoelectricity by self-assembled highly porous perovskite–polymer composite films to enable the internet of things[J]. Journal of Materials Chemistry A, 2020, 8(27): 13619-13629.

[6]. Mahanty B, Ghosh S K, Garain S, et al. An effective flexible wireless energy harvester/sensor based on porous electret piezoelectric polymer[J]. Materials Chemistry and Physics, 2017, 186: 327-332.

[7]. Abolhasani M M, Naebe M, Hassanpour Amiri M, et al. Hierarchically structured porous piezoelectric polymer nanofibers for energy harvesting[J]. Advanced Science, 2020, 7(13): 2000517.

[8]. Ye S, Cheng C, Chen X, et al. High-performance piezoelectric nanogenerator based on microstructured P (VDF-TrFE)/BNNTs composite for energy harvesting and radiation protection in space[J]. Nano Energy, 2019, 60: 701-714.

[9]. Chen X, Li X, Shao J, et al. High-performance piezoelectric nanogenerators with imprinted P (VDF-TrFE)/BaTiO3 nanocomposite micropillars for self-powered flexible sensors[J]. Small, 2017, 13(23): 1604245.